Thermal-hydraulic simulation of the CFETR TF coil operation during a plasma scenario: Gandalf-Fluent and 4C code-to-code comparison

(Article begins on next page)
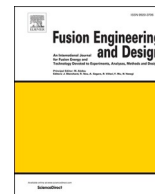
19 December 2024

# Thermal-hydraulic simulation of the CFETR TF coil operation during a plasma scenario: Gandalf-Fluent and 4C code-to-code comparison

Xinghao Wen [a], Roberto Bonifetto [c,*], Junjun Li [b], Roberto Zanino [c], Yu Wu [b], Xiang Gao [b]

[a] School of Carbon Neutrality Science and Engineering, Anhui University of Science and Technology, Hefei, Anhui 230031, China
[b] Institute of Plasma Physics, Chinese Academy of Sciences, Hefei, Anhui 230031, China
[c] NEMO Group, Dipartimento Energia, Politecnico di Torino, Torino 10129, Italy

**ABSTRACT**

Within the framework of the comprehensive research facility for fusion technology (CRAFT) activities, a prototype toroidal field (TF) coil has been designed and will be manufactured at the Institute of Plasma Physics, Chinese Academy of Sciences (ASIPP), in Hefei. The main purpose is to develop and validate the manufacturing technologies of the large-scale superconducting coils of the China Fusion Engineering Test Reactor (CFETR). To ensure the safe operation of the CFETR device, the Gandalf-Fluent tool and the 4C code are employed to evaluate the performance of the superconducting magnets, and their thermal-hydraulic simulation results are compared with each other. The comparison shows that the thermal coupling between turns and pancakes and the transient model of the thermal coupling to the casing structures, accounted for in 4C but neglected in Gandalf-Fluent, have a significant effect on the temperature profile. Then a detailed reassessment of the minimum temperature margin ($\Delta T_{\mathrm{mar}}^{\min}$) is carried out using the 4C code. The results show that the $\Delta T_{\mathrm{mar}}^{\min}$ is $\sim 1.0$ K (if a realistic value for the inter-turn and inter-pancake coupling parameter is assumed), lower than the design requirement of 1.2 K, and it deserves the attention of the designers.

## 1. Introduction

The China Fusion Engineering Test Reactor (CFETR) toroidal field (TF) coil system consists of sixteen d-shaped identical superconductive magnets arranged in toroidal array. The magnetic field of the CFETR on the magnetic axis is 6.5 T, and the peak magnetic field of the TF coils is up to 14.4 T. The engineering design of the TF coils was carried out from 2017 to 2020 [1], and a prototype TF coil will be manufactured and tested at ASIPP in the comprehensive research facility for fusion technology (CRAFT) [2] framework. The main purpose is to develop and validate the manufacturing technologies of the large-scale superconducting coils of the fusion reactor.

To save costs, three kinds of materials are used for the TF coil, see Fig. 1(b). High-performance Nb$_3$Sn is used for the double-pancake winding of the high field (HF) region (or sub-coil), ITER-like Nb$_3$Sn is used for the single-pancake winding of the medium field (MF) region, and NbTi is selected for the double-pancake winding of the low field (LF) region [3], see also Fig. 1(c). All the sub-coil conductors are circle-in-square cable-in-conduit conductors (CICC) with a central pressure relief channel, and the cable layout and the dimensions of the three types of conductor are designed to be the same as reported in Fig. 1 (a). The stainless steel casing is actively cooled by a set of 68 parallel casing cooling channels, 32 in the inboard leg and 32 in the outboard one, with the He inlet at the magnet bottom and its outlet at the top.

The overview and main characteristics of the TF coil is illustrated in Fig. 2(a). The design of this hybrid magnet also faces big challenges for the winding pack (WP) fabrication technology. For example, a gap of 10 mm increasing up to 120 mm will be drawn between the sub-coils to arrange the helium inlet and outlet tubes, as shown in Fig. 2(b). The detailed engineering design of the TF coil can be found in [3].

To ensure the safe operation of the CFETR, the Gandalf-Fluent tool [4] is used to evaluate the performance of the TF coils, and the relevant results were first published in 2021 [4]. However, the accuracy of Gandalf-Fluent coupled tool has not yet been benchmarked against another reference code or validated against experimental data. This paper aims at verifying the Gandalf-Fluent code by comparing its results to those of the state-of-the-art 4C code [5,6].

The Gandalf code [7], is a commercial, easy to handle and well-established numerical tool for the 1D thermal hydraulic analysis of a single CICC. It does not model the transverse heat diffusion, but it can

be easily customized through external subroutines [8]. The Gandalf code has already been applied to the quench analysis of the ITER TF coils [9], the computation of the temperature margin of the JT60SA TF coils [8] and the analysis of the CFETR TF coils in normal [4] and off-normal [10] operation.

The 4C code [5,6] is the state-of-the-art tool for the thermal hydraulic analysis of a whole superconducting magnet system, with particular reference to: (1) the WP, (2) the structure (in the case of the TF coils) and (3) the cryogenic circuits. During the last ~12 years, the 4C code has been successfully validated against experimental data [11–16], also predictively [14,16] and applied to the ITER TF coil fast discharge [17] and cool-down [18], the EU DEMO [6], JT-60SA [19], KSTAR [20] and EAST magnet systems [21].

## 2. Thermal-hydraulic model of a CFETR TF coil

The central channel and the bundle area of the cable are modeled by two parallel channels where the supercritical helium flows, with heat and mass transfer between the two. In each channel, the pressure drop $\Delta P$ can be expressed as

$$\Delta P = f \frac{m^2}{\rho} \frac{U}{8A^3} L \tag{1}$$

where $f$ is the friction factor, $U$ is the helium wetted perimeter, $m$ is the mass flow rate, $\rho$ is the helium density, $A$ is the flow area and $L$ is the hydraulic length.

The friction factor in the bundle region $f_b$ and the central channel $f_c$ are given by [22,23]

$$f_b = \frac{1}{\nu^{0.742}} \left( \frac{19.5}{Reb^{0.7953}} + 0.0231 \right) in\,the\,bundle\,region \tag{2}$$

$$f_c = \frac{0.3024}{Rec^{0.0707}} in\,the\,central\,channel \tag{3}$$

where $\nu$ is the void fraction and $Reb$ and $Rec$ are the Reynolds number of bundle and central channel respectively. Note that the friction factor correlation for the central channel is developed for an outer diameter of 12 mm, while the channel in the CFETR TF coils will have a 10/12.5 mm inner/outer diameter, see again Fig. 1(a).

The critical current density of the high-performance $Nb_3Sn$ and ITER-like $Nb_3Sn$ is computed according to the scaling law in [24]. The expected effective strain used in the $Nb_3Sn$ critical current density is assumed to be −0.60 %, from [3]. The critical current density of the NbTi is computed according to the scaling law in [25]. The scaling law parameters of the $Nb_3Sn$ and NbTi strands are shown in Table 1.

The magnetic field on the conductor axis at each axial location along the cooling path is used to evaluate the temperature margin ($\Delta T_{mar}$), which is defined as the difference between the current sharing temperature ($T_{cs}$) and the operating temperature ($T_{op}$). For the sake of simplicity, the magnetic field generated by central solenoid and poloidal field coils and plasma on the TF coils is neglected, so it can be considered that the magnetic field distribution along the cooling channels is constant during the whole simulation.

The main differences between the Gandalf and 4C models are as follows:

The inter-turn and inter-pancake thermal coupling are not included in the Gandalf model, while it is accounted for in the 4C code. Here, the insulation between the turns and pancakes is considered as a thermal resistance [26], and the heat transfer coefficient is defined as

$$\text{Heat transfer coefficient} = M_{IT,IP}, \; k/\delta \tag{4}$$

where $k$ is the thermal conductivity of insulating material and $\delta$ is the insulation thickness between two neighboring jacket sides. The $M_{IT,IP}$ is a fitting parameter that needs to be calibrated by means of suitable experiments, being it related to the uncertainty on the thickness and thermophysical properties of each layer of the insulation, including also resin layers after the impregnation [19]. In [19] $M_{IT,IP}$ = 0.2 was
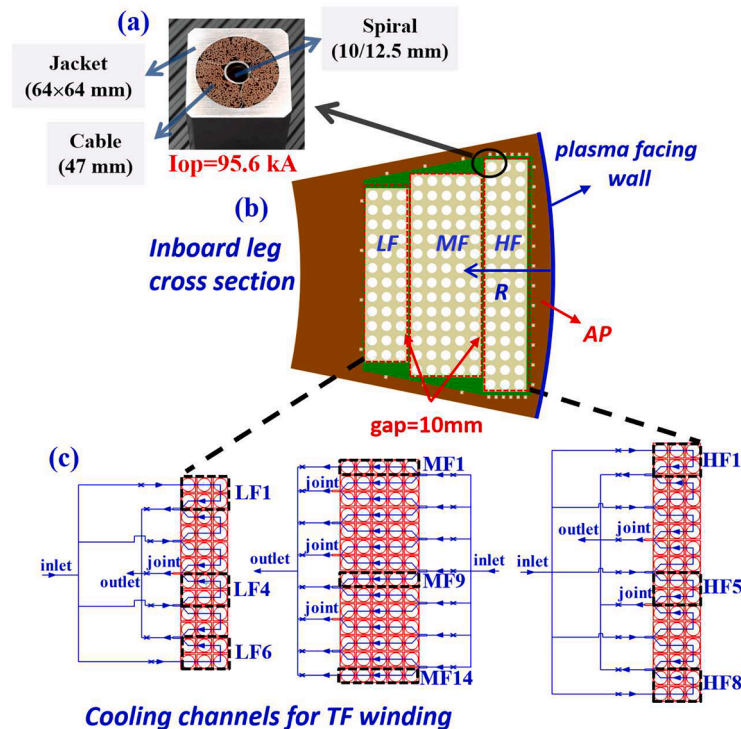


**Fig. 1.** In (a) the cross section of the conductor is shown; all the sub-coil conductors are circle-in-square CICCs with a central pressure relief channel. In (b) the cross section of the inboard leg is given. In (c) the cooling paths of the sub-coils are reported: for the HF and LF sub-coils, each pair of neighboring pancakes is cooled in series, while for the MF sub-coil each pancake is cooled by one hydraulic channel. (Partly reproduced from [4]).
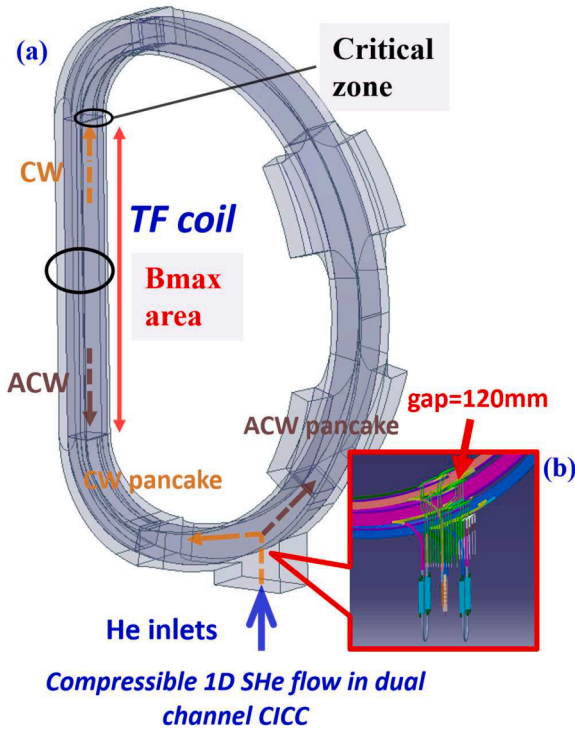
**Fig. 2.** Overview and main characteristics of CFETR TF coil. Each helium inlet feeds two adjacent cooling channels, hence the helium flow direction in adjacent cooling channels is opposite: one is clockwise (CW), the other is anticlockwise (ACW), as shown in (a). In (b) a gap of 10 mm increasing up to 120 mm will be drawn between the sub-coils to arrange the helium inlet and outlet tubes. (Reproduced from [4]). The He inlet and outlet of the winding is at the magnet bottom, and the He inlet of the casing is at the magnet bottom and its outlet at the top.

**Table 1**
Scaling law parameters of Nb$_3$Sn strand and NbTi strand.

|  | High-Jc Nb$_3$Sn | ITER Nb$_3$Sn |  | NbTi |
|---|---|---|---|---|
| $C_{a1}$ | 38.00 | 49.00 | $\alpha$ | 1 |
| $C_{a2}$ | 2.6 | 0.300 | $\beta$ | 1.54 |
| $\varepsilon_{0,a}$ | 0.24 % | 0.312% | $\gamma$ | 2.1 |
| $\varepsilon_m$ | 0.00 | 0.00 | $B_{c20}$ (T) | 14.61 |
| $\mu_0 H_{c2m}(0)$ (T) | 29.17 | 33.24 | $T_{c0}$ (K) | 9.03 |
| $T_{cm}$ (K) | 15.92 | 16.34 | $C_0$ (A·T) | 168,512 |
| $C_1$ (A·T) | 72,700 | 32,300 |  |  |
| $p$ | 0.50 | 0.593 |  |  |
| $q$ | 2.00 | 2.156 |  |  |

obtained as best-fitting parameter comparing the simulations with the experimental data in the case of JT-60SA, and same fitting parameter is computed in [20] for KSTAR PF1 coil. More recently, also in the case of the ITER CS module tests [27] an average value of 0.2 was estimated experimentally for $M_{IT}$ and $M_{IP}$. The value of 0.2 for this parameter can therefore be considered typical for the coils without radial plates.

Both Fluent and 4C use finite element methods to build the casing model. The casing is divided into a limited number of segments in the poloidal direction and every segment is approximated with a 2D finite-element model. The commercial Fluent tool is coupled to the Gandalf code: it runs once before Gandalf, to provide a constant input to it. In the 4C model, the shareware FreeFem++ [28] is employed, which is run in parallel (co-simulation) to the M&M code [26] modeling the WP, and the data can be exchanged at each time step.

## 3. Simulation setup

The reference plasma scenario is characterized by a pulse length of 5000 s, with a plasma current of 14 MA [4]. The deposited nuclear heat load decreases exponentially along the radial direction from TF coil inner edge.

$$P_{nh}(r) = P_{nh,max} \exp(-7r) \tag{5}$$

where $P_{nh,max}$ is the maximum deposition power density (in W/m$^3$), and $r$ (in m) is the radial distance from the plasma facing wall of the magnet, see Fig. 1(b).

The distribution of the average nuclear heat load along the D shape of the TF coil is shown in Fig. 3. The assumed net thermal power production of the CFETR following the plasma burn giving the nuclear heating is 1 GW. A constant nuclear heat load is applied to the WP and casing during the plasma burn (70–5000 s), while during the plasma current ramp-up (0–70 s) and ramp-down (5000–5300 s), the nuclear heat load is applied proportionally to the plasma current. The dwell period (without nuclear heat load deposition) will then last 3000 s.

The thermal-hydraulic boundary conditions (BCs) are kept fixed in the simulation: inlet pressure ~0.6 MPa, inlet temperature ~4.2 K, and outlet pressure such as to guarantee a mass flow rate ~0.012 kg/s in each cooling path during the dwell [3]. The main conductor parameters are shown in Table 2.

The 4C analysis has been carried out to assess when fully periodic thermal-hydraulic behavior would have been obtained. Fig. 4 shows that it is already repetitive after the first pulse. The HF1 outlet temperature is higher than HF5 because the WP is compressed inward by the centering force during normal operation, and a gap up to 3 mm appears between the coil case and the inner side of the HF WP [2]. Hence the nuclear heat load on the coil case side facing the plasma that cannot be taken away by the casing cooling circuits will be transferred to the side pancakes (namely, HF1 and HF8), causing the outlet temperature of the HF1 to be higher than that of HF5.

## 4. Results

### 4.1. Code comparison without structure model

The code-to-code comparison results reported in this part are obtained without coupling the WP model to the structure one. The temperature profiles at the end of plasma calculated by the two codes show a good consistency if the coupling parameter $M_{IT,IP}$ in the 4C code is set to 0, i.e. assuming the turns and pancakes are adiabatic to each other, see the black and blue solid lines in Fig. 5 and Fig. 6. The difference between the conductor temperature computed by the two codes at the maximum magnetic field ($B_{max}$) location is only ~0.06 K, which is considered acceptable. The conductor temperature distribution at 5000 s is reported
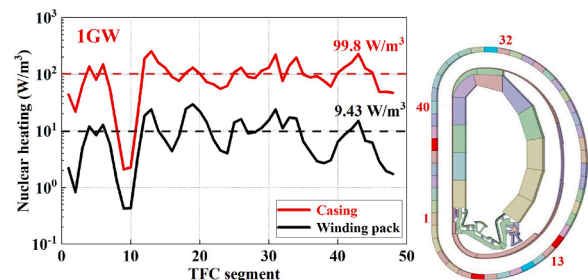


**Fig. 3.** The distribution of nuclear heat load along D shape of the TF coil is given on the left. The numbering schematic used to define the nuclear heating distribution is shown on the right. The nuclear heating is the lowest below the divertor due to the insertion there, in the CFETR, of a new blanket module concept that increases the tritium breeding ratio (TBR) and reduces the nuclear heat load of the TF coils.

**Table 2**
Main conductor and strand parameters relevant for the present study.

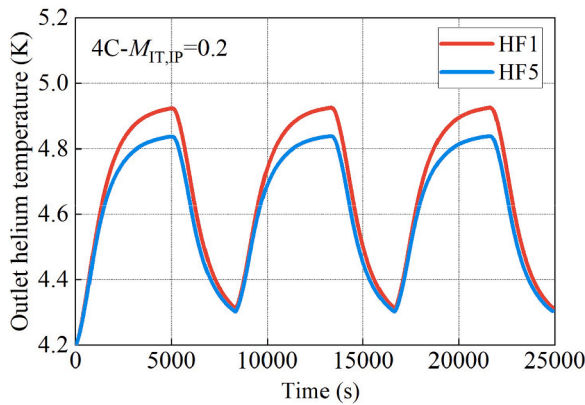| | LF | MF | HF |
|---|---|---|---|
| SC material | NbTi | ITER Nb$_3$Sn | RRP Nb$_3$Sn |
| Strand Dia. (SC, Cu in triplet and Cu in core) (mm) | 1.00 | | |
| Cu:Non-Cu | 1.60 | 1.00 | 1.00 |
| B$_{max}$ (T) | 5.5 | 10.6 | 14.5 |
| Number of SC | 900 | | |
| Number of Cu | 522 | | |
| Number of strands | 1422 | | |
| Conductor width (mm) | 64.0 × 64.0 | | |
| Cable Dia. (mm) | 47.0 | | |
| Dia. of central spiral (mm) | 12.5/ 10.0 | | |
| Operation current (kA) | 95.6 | | |



**Fig. 4.** Evolution of the outlet helium temperature computed by 4C for HF1 and HF5 cooling channels, with coupling parameter $M_{IT,IP} = 0.2$.
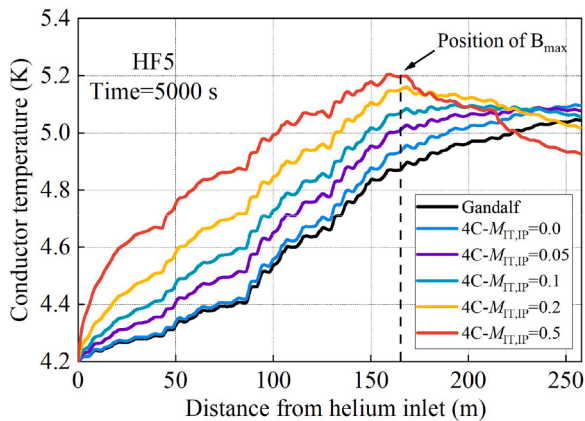


**Fig. 5.** Computed distribution of the temperature along the HF5 cooling channel at the end of plasma, without structure model.

in Fig. 5: the outlet temperature there is compliant with its evolution reported in Fig. 6, at that time.

Then, a parametric study is performed using the 4C code to assess the effect of the coupling parameter $M_{IT,IP}$ on the temperature profile, showing that this effect is significant. While $M_{IT,IP}$ increases, the temperature peak moves towards the middle of the cooling channel length. The reason is that the fresh helium flowing in the first pancake is (pre-) heated by the warm helium flowing back in the second pancake. If $M_{IT,IP}$ is set to the typical value of 0.2, the temperature difference between the two codes reaches 0.3 K in the critical, high-field zone. As the $T_{cs}$ distribution along the cooling channels is constant during the whole
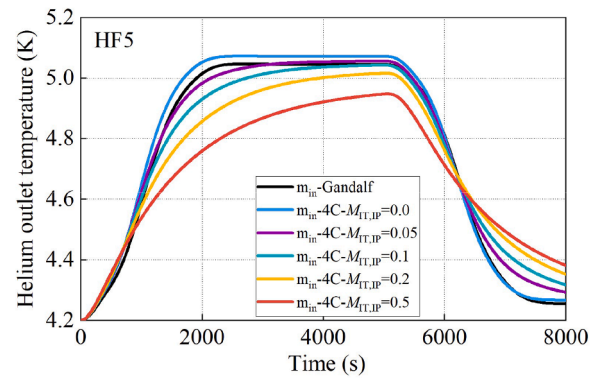


**Fig. 6.** Computed evolution of helium outlet temperature of the HF5 cooling channel, without structure model.

simulation, it means that neglecting the thermal coupling between the turns and pancakes will cause a non-conservative overestimation of the $\Delta T_{mar}$ in the critical zone.

The inlet and outlet mass flow rate evolution calculated by the two codes are in good agreement (with the 4C coupling parameter $M_{IT,IP} = 0$), as shown by the black and blue lines in Fig. 7. Increasing $M_{IT,IP}$, i.e. causing more heat to be transferred back by conduction towards the helium inlet, leads to a decrease in the computed inlet mass flow rate during the plasma, see the solid lines in Fig. 7.

The pressure drop (not shown) given in input to the two codes is perfectly consistent, as expected, because the same friction factor formulas are used in the simulation.

### 4.2. Code comparison with structure model

The Fluent tool is used to model the heat conduction in the structures with finite element methods before running the Gandalf simulation. In the steady state Fluent model, the WP external boundaries in contact with the structures are assumed to be at 4.2 K, and the structure temperature distribution is computed. This is then used to provide constant thermal BCs to the Gandalf simulation of the transient in the WP [4]. On the other hand, in the 4C model the shareware FreeFem++ tool [28], also based on finite elements, is employed. It solves the transient heat conduction problem in selected 2D cross-sections of the casing and runs in parallel (co-simulation) to the WP model, so that the BCs are updated and exchanged at each time step, taking into account the thermal feedbacks due to the transient scenario.

The results of Gandalf-Fluent model and 4C model are compared, showing the effect of the coupling parameter $M_{IT,IP}$ in Fig. 8. The qualitatively different behavior shown in the $M_{IT,IP} = 0$ case is due to the fact that in the 4C model the thermal feedbacks exchanged between the
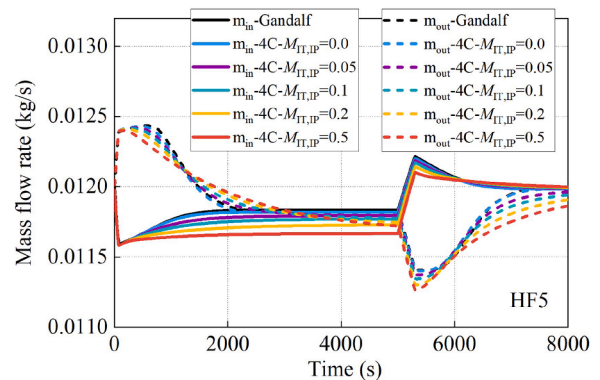


**Fig. 7.** Computed evolution of mass flow rate at the inlet and outlet of the HF5 cooling channel, without structure model.
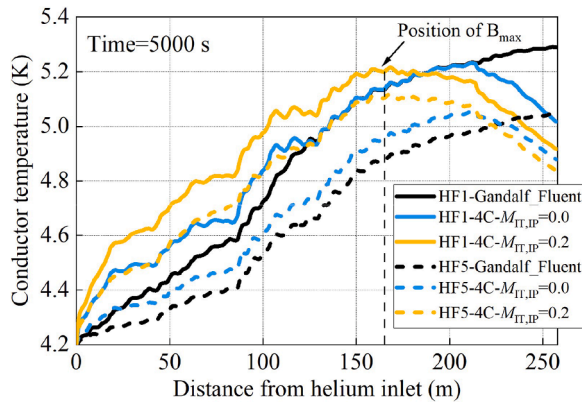
**Fig. 8.** Temperature profile along the HF1&HF5 cooling channel at the end of plasma, with coupling between winding and structures.



**Fig. 9.** Computed distribution of the temperature along selected cooling channels with coupling parameter $M_{IT,IP} = 0.2$.

casing and WP allow capturing the heating of first turn (0.0–43.3 m) of HF cooling channels by the last turn (214.9–258.2 m) (which is therefore cooled); this heat transfer occurs by conduction through the insulation that is inserted between the HF sub-coil and MF sub-coil. Actually, the major differences arise in the turns of the WP in contact with the structures, namely the first three turns of the side hydraulic channels (e. g. HF1), and the first and last turn of all hydraulic channels: actually, in HF5 the temperature distributions computed by Gandalf-Fluent and 4C differ in the first turn, then the offset is kept constant in the central turns not in contact with the structures, and then is again different in the last turn. The latter in the 4C code is cooled by the structures, in turn cooled by the cold He entering the first turn close to it. This effect is indeed not visible in Fig. 5 (e.g. for the case $M_{IT,IP} = 0$), where the structure model is not included. The Gandalf-Fluent assumption of keeping the WP temperature constant at 4.2 K for the structure analysis was considered conservative before, because it overestimates the temperature difference between the casing and WP. But this code-to-code comparison shows that it needs to be reconsidered, since the coupling between the WP and structures bridges heat exchange of first and last turns of HF sub-coil cooling channels, as shown by the 4C code results.

### 4.3. Thermal analysis of TF coil using the 4C code

The code-to-code comparison shows that both the thermal coupling between turns and pancakes and the thermal feedbacks from the structure temperature evolution, accounted for in 4C code but neglected in Gandalf-Fluent tool, have a significant effect on the temperature profile. This may affect the design of the CFETR TF coil cooling. Therefore, a detailed reassessment of the minimum $\Delta T_{mar}$ ($\Delta T_{mar}^{min}$) in TF coil during normal operation is performed using the 4C code, together with the sensitivity analysis to the coupling parameter $M_{IT,IP}$ on the $\Delta T_{mar}^{min}$. The radiative heat thansfer with the thermal shield, whose temperature is set at 80 K, is also accounted for by the 4C code, and the coupling parameter $M_{IT,IP} = 0.2$ is adopted as reference value.

The resulting temperature profiles along selected cooling channels are reported in Fig. 9, showing that the temperature rise of the side channels is higher than that of the central channels. The reason is that they have an entire pancake side in contact with the casing from which they are heated, while in the central channels only the sub-coil inner-most and outermost turns are in contact with the casing. Moreover, a gap between the casing and the inner side of the HF sub-coil is considered, due to the electro-magnetic force pushing outwards the WP, that inhibits the direct heat transfer by conduction of the nuclear heat deposited in the plasma-facing side of the casing to the innermost turns of the HF sub-coil. Therefore, some of the heat load on the casing that can't be removed by the casing cooling channels is transferred to the side pan-cakes only. The temperature rise of the HF sub-coil is larger than that of
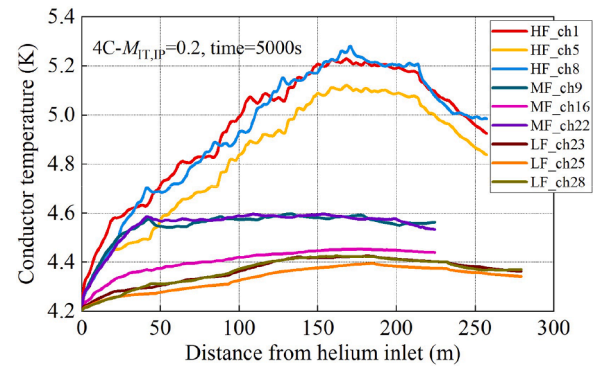
the MF and LF sub-coils, because the nuclear heat load decreases rapidly from the plasma side along the magnet cross section. The peaked behavior of the HF coil is due to its double-pancake winding topology, see again Fig. 1(c): the cold He injected at the outer radius of the sub-coil is heated while moving towards the inner (plasma) side, and then when in the second pancake it moves outwards towards the outlet it is partially recooled by the cold He in the neighboring pancakes. The same effects is barely visible in the LF sub-coil, also double-pancake wound, because of the much lower nuclear heat load there. On the other hand, the MF sub-coil is single-pancake wound; therefore, its temperature distribustion is monotonically increasing in the first turns, and then as the nuclear heat load decreases (because the He, entering at the sub-coil inner radius, is moving outwards) the temperature profile flattens.

The computed $\Delta T_{mar}^{min}$ decreases as the coupling parameter $M_{IT,IP}$ increases, see Fig. 10. For the reference value $M_{IT,IP} = 0.2$, the $\Delta T_{mar}^{min}$ is ~ 1.0 K, which is lower than the design limit of 1.2 K. Even for $M_{IT,IP} = 0$, the $\Delta T_{mar}^{min}$ is still below the design requirement, as opposed to the Gandalf results, because of the non conservative assumptions made in the Gandalf-Fluent tool, where the thermal coupling between the WP and the casing is not modelled. This will possibly drive changes of the CFETR TF coil cooling design (e.g., reducing the cooling channel length), or of the cooling parameters (e.g., increasing the mass flow rate or reducing the inlet temperature).

### 5. Conclusions and perspective

The thermal-hydraulic behavior of the TF coils of the CFETR during a plasma scenario is analyzed here with the Gandalf-Fluent and 4C codes.
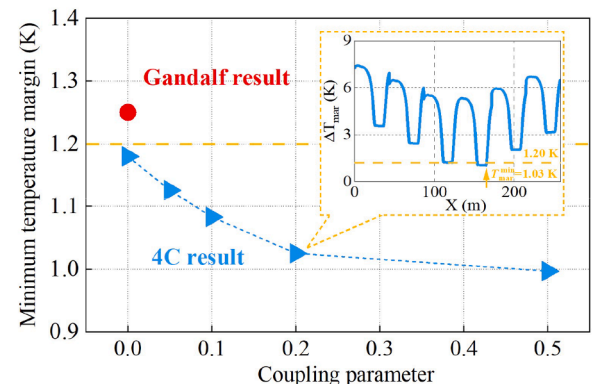


**Fig. 10.** Minimum temperature margin during the reference scenario computed by different values of the coupling parameter $M_{IT,IP}$. The yellow dashed line represents the design requirement of $\Delta T_{mar}^{min}$. The inset shows the computed distribution of the temperature margin along the cooling channels with coupling parameter $M_{IT,IP} = 0.2$.

Firstly, the two codes are compared in the case without the structure model. The comparison shows a good consistency between the two codes when the turns and pancakes are considered adiabatic in 4C, as intrinsic to the Gandalf model. However, this thermal coupling has a significant effect on the temperature profile, and the temperature difference between the two codes reaches 0.3 K in the critical zone, if that coupling is accounted for in the 4C code.

Then, the results of Gandalf-Fluent and 4C simulations including the structures are compared, showing that the coupling between the WP and structure bridges the inter-turn heat exchange, increasing the difference between the temperature profiles computed by the two codes. Therefore, this code-to-code comparison highlighted the importance of some heat transfer mechanisms, namely the thermal coupling between turns and pancakes and the thermal feedbacks from the structure temperature evolution on the WP. They do not apply only to the CFETR TF coils, but can also have an impact on the design of cooling channels and cooling parameters of other superconducting magnets.

Finally, a detailed reassessment of the $\Delta T_{mar}^{min}$ in the TF coil is performed using the 4C code. The results show that the computed $\Delta T_{mar}^{min}$ decreases as the inter-turn and inter-pancake thermal coupling increases. The $\Delta T_{mar}^{min}$ falls below the design requirement, and it deserves the attention of the designers.

In the future, effective strategies to mitigate the reduction of the $T_{mar}^{min}$ will be investigated with the 4C code, such as increasing the mass flow rate and decreasing the operating temperature.

## CRediT authorship contribution statement

**Xinghao Wen:** Software, Writing – original draft. **Roberto Bonifetto:** Methodology, Supervision, Writing – review & editing. **Junjun Li:** Conceptualization, Supervision, Funding acquisition. **Roberto Zanino:** Project administration. **Yu Wu:** Project administration. **Xiang Gao:** Project administration.

## Declaration of Competing Interest

The authors declare that they have no known competing financial interests or personal relationships that could have appeared to influence the work reported in this paper.

## Data availability

No data was used for the research described in the article.

## Acknowledgements

## References

[1] J.X. Zheng, Y.T. Song, F. Liu, X.F. Liu, K. Lu, L. Zhu, W.W. Xu, G. Shen, C. Fang, C. Li, M. Li, H.Y. Liu, Progress in engineering design of CFETR toroidal field superconducting magnet, Fus. Eng. Des. 177 (2022), 113063.

[2] X.G. Liu, F. Wu, Z.L. Wang, G.Q. Li, X.J. Liu, H. Li, J.J. Li, Y. Ren, Y. Wu, X. Gao, Progress in the conceptual design of the CFETR toroidal field coil with rectangular conductors, Nuclear Fus. 60 (4) (2020) 10.

[3] Y. Wu, J.G. Li, G. Shen, J.X. Zheng, X.G. Liu, F. Long, C. Dai, X.F. Liu, Y. Shi, J. J. Liu, Q.W. Hao, Y.L. Hu, Y.Z. Xiao, W. Wen, X.W. Yu, C. Fang, J. Wei, L.N. Zhu, H. X. Han, Preliminary design of CFETR TF prototype coil, J. Fus. Energy 40 (1) (2021) 14.

[4] X.H. Wen, J.J. Li, A.G. Sang, Y. Ren, X.G. Liu, Y. Wu, X. Gao, Thermal-hydraulic analysis of the CFETR TF coils when subject to nuclear heat load, Fusion Eng. Des. 173 (2021), 112850.

[5] L. Savoldi Richard, F. Casella, B. Fiori, R. Zanino, The 4C code for the cryogenic circuit conductor and coil modeling in ITER, Cryogenics 50 (2010) 167–176 (Guildf).

[6] R. Zanino, R. Bonifetto, O. Dicuonzo, L. Muzzi, G.F. Nallo, L.S. Richard, S. Turtù, Development of a thermal-hydraulic model for the european DEMO TF Coil, IEEE Trans. Appl. Supercond. 26 (3) (2016), 4201606.

[7] L. Bottura, A numerical model for the simulation of quench in the ITER magnets, J. Comput. Phys. 125 (1996) 26–41.

[8] B. Lacroix, C. Portafaix, P. Hertout, S. Nicollet, L. Zani, P. Barabaschi, R. Villari, Thermo-hydraulic analyses associated with the design of JT-60SA TF coils development and validation of the TACOS/TEXTO tool, Adv. Cryog. Eng. 1218 (2010) 471–479.

[9] S. Nicollet, D. Bessette, D. Ciazynski, M. Coatanéa-Gouachet, J.L. Duchateau, B. Lacroix, F. Rodriguez-Mateos, Thermal behavior and quench of the ITER TF system during a fast discharge and possibility of a secondary quench detection, IEEE Trans. Appl. Supercond. 22 (3) (2012), 4704304.

[10] X.H. Wen, J.J. Li, A.G. Sang, Y. Ren, X.G. Liu, X. Gao, et al., Quench analysis of the CFETR TF coil using the gandalf code, IEEE Trans. Appl. Supercond. 31 (3) (2021) 5.

[11] R. Zanino, R. Bonifetto, R. Heller, L.S. Richard, Validation of the 4C thermal-hydraulic code against 25 kA safety discharge in the ITER toroidal field model coil (TFMC), IEEE Trans. Appl. Supercond. 21 (3) (2011).

[12] R. Bonifetto, A. Kholia, B. Renard, K. Riße, L. Savoldi Richarda, R. Zanino, Modeling of W7-X superconducting coil cool-down using the 4C code, Fus. Eng. Des. 86 (2011) 1549–1552.

[13] R. Bonifetto, T. Isono, N. Martovetsky, L. Savoldi Richarda, R. Zanino, Analysis of quench propagation in the ITER central solenoid insert (CSI) coil, IEEE Trans. Appl. Supercond. 27 (4) (2017), 4700308.

[14] R. Zanino, R. Bonifetto, A. Brighenti, T. Isono, H. Ozeki, L. Savoldi Richarda, Prediction, experimental results and analysis of the ITER TF insert coil quench propagation tests, using the 4C code, Supercond. Sci. Technol. 31 (2018), 035004.

[15] R. Bonifetto, F. Casella, L. Savoldi Richard, R. Zanino, Dynamic modeling of a supercritical helium closed loop with the 4C code, AIP Conf. Proc. 1434 (2012) 1743.

[16] R. Zanino, R. Bonifetto, C. Hoa, L. Savoldi Richard, Verification of the predictive capabilities of the 4C code cryogenic circuit model, AIP Conf. Proc. Adv. Cryogenic Eng. 1573 (2014) 1586–1593.

[17] L. Savoldi Richard, D. Bessette, R. Bonifetto, R. Zanino, Parametric analysis of the ITER TF fast discharge using the 4C code, IEEE Trans. Appl. Supercond. 22 (3) (2012), 4704104.

[18] R. Bonifetto, F. Buonora, L.S. Richard, R. Zanino, 4C code simulation and benchmark of ITER TF magnet cool-down from 300K to 80 K, IEEE Trans. Appl. Supercond. 22 (3) (2012), 4902604.

[19] R. Bonifetto, L. Savoldi Richard, R. Zanino, Thermal-hydraulic analysis of the JT-60SA central solenoid operation, IEEE Trans. Appl. Supercond. 29 (5) (2019), 4201005.

[20] L. Savoldi Richard, R. Bonifetto, Y. Chu, A. Kholia, S.H. Park, H.J. Lee, R. Zanino, 4C code analysis of thermal-hydraulic transients in the KSTAR PF1 superconducting coil, Cryogenics 53 (2013) 37–44 (Guildf).

[21] J.J. Li, R. Bonifetto, L. Savoldi Richard, R. Zanino, Analysis of AC losses in the EAST superconducting magnets using the 4C Code, IEEE Trans. Appl. Supercond. 26 (4) (2016), 4204605.

[22] N. Peng, L.Q. Liu, L. Serio, L.Y. Xiong, L. Zhang, Thermo-hydraulic analysis of the gradual cool-down to 80K of the ITER toroidal field coil, Cryogenics 49 (2009) 402–406 (Guildf).

[23] S. Nicollet, J.L. Duchateau, H. Fillunger, A. Martinez, S. Parodi, Dual channel cable in conduit thermohydraulics: influence of some design parameters, IEEE Trans. Appl. Supercond. 10 (1) (2000) 1102–1105.

[24] Godeke, B. ten Haken, H.H.J ten Kate, D.C. Larbalestier, A general scaling relation for the critical current density in Nb$_3$Sn, Supercond. Sci. Technol. 19 (10) (2006) 100–116.

[25] L. Bottura, A practical fit for the critical surface of NbTi, IEEE Trans. Appl. Supercond. 10 (1) (2000) 1054–1057.

[26] L. Savoldi, R. Zanino, M&M: multi-conductor Mithrandir code for the simulation of thermal-hydraulic transients in superconducting magnets, Cryogenics 40 (3) (2000) 179–189 (Guildf).

[27] Zappatore, R. Bonifetto, N. Martovetsky, R. Zanino, Development and validation of the 4C thermal–hydraulic model of the ITER central solenoid modules, Cryogenics 127 (2022), 103552 (Guildf).

[28] Hecht, "New development in FreeFem++," *J. Numer. Math.*, 2012, 20, 251–266.

**XINGHAO WEN** was born in Henan, China, in 1994. He received the B.S. degree in Electrical and Power Engineering from the China University of Mining and Technology, in 2017, and the Ph.D. degree in Nuclear Science and Technology, University of Science and Technology of China, Hefei, in 2023. He is currently an Assistant Professor in the School of Carbon Neutrality Science and Engineering, Anhui University of Science and Technology. His-current research interests include thermal-hydraulic and cooling design of fusion superconducting magnet.

**ROBERTO ZANINO** (Senior Member, IEEE) received the M.*Sc.* degree in nuclear engineering and the Ph.D. degree in energetics from Politecnico di Torino (PoliTo), Turin, Italy.

He has been a Professor of nuclear engineering with the Energy Department at PoliTo since 2001, and the Founder and Coordinator of the Nuclear Engineering Modeling (NEMO). He has authored or coauthored over 200 papers that appeared in international journals devoted to computational modeling in the fields of relevance for nuclear fusion (superconducting magnets and cryogenics, plasma–wall interactions, and high heat flux components), nuclear fission (Gen-IV lead-cooled fast reactors), and concentrated solar power.

Prof. Zanino is a member of the EURATOM Science and Technology Committee as well as the Italian Academy of Engineering and Technology, and also the Vice President of the Italian Consortium for Research in Nuclear Technologies (CIRTEN).

**ROBERTO BONIFETTO** (Member, IEEE) received the B.S. and M.S. degrees in energy and nuclear engineering, and the Ph.D. degree in energetics from the Politecnico di Torino, Turin, Italy, in 2008, 2010, and 2014, respectively. He has been an Associate Professor of nuclear engineering with the Energy Department, Politecnico di Torino, since 2021. He has authored or coauthored over 60 papers on international journals, concerning the development, validation, and application of computational tools for the modeling of nuclear fusion and fission devices, the computational fluid dynamics analysis of high-heat fusion components, and the tritium extraction from the EU DEMO Breeding Blanket. He is currently involved, in particular, in the design of the Italian DTT and EU DEMO magnet systems, being a project leader of the DTT thermal shield, since 2022.

Prof. Bonifetto is also a member of the American Nuclear Society and of the Associazione Italiana Nucleare, and regularly serves as a Referee for the IEEE TRANSACTIONS ON APPLIED SUPERCONDUCTIVITY. He received the IEEE Graduate Study Fellowship in applied superconductivity, in 2014, and the European Nuclear Education Network Association Ph.D. Prize, in 2013. He was awarded a EUROfusion Postdoctoral Fellowship and a EUROfusion Engineering Grant, in 2014 and 2016, respectively.

**YU WU** was born in Anhui, China, 1964. In 1985, he received his B.S. degree in Reactor Engineering from Xi'an Jiaotong University. He is currently a Professor and experimental scientist in the Institute of Plasma Physics, Chinese Academy of Sciences. His-ongoing researches focus on the Applied superconductivity and cryogenics, Superconductor design and manufacturing, superconducting magnet design and manufacturing.

**JUNJUN LI** was born in Shanxi, China, in 1984. He received the B.S. degree in Applied Physics from the Shanxi University, in 2007, and the Ph.D. degree in Plasma Physics from the Institute of Plasma Physics, Chinese Academy of Sciences, Hefei, in 2012. He is currently a associate Researcher in the Institute of Plasma Physics, Chinese Academy of Sciences. His-current research interests thermal hydraulic modeling of superconducting magnet systems for fusion reactors.

**XIANG GAO** was born in Tianchang, China, in 1965. He received the B.S. degree in Laser Optics from the Southeast University, in 1985, the M.S. degrees in Plasma Physics from the Institute of Plasma Physics, Chinese Academy of Sciences, Hefei, in 1990, and the Ph.D. degrees in Plasma Physics and Controlled Fusion from the Institute of Plasma Physics, Chinese Academy of Sciences, Hefei, in 1997. He is currently a Professor in the Institute of Plasma Physics, Chinese Academy of Sciences. His-current research interests include key issues for long-pulse high beta-N operation, formation and maintenance of internal transport barrier (ITB), and experimental study of pedestal turbulence with the Experimental Advanced Superconducting Tokamak.